

FINAL TECHNICAL REPORT

AWARD# 06HQGR0067

**TITLE: INVESTIGATION OF LARGE MAGNITUDE PALEOLIQUEFACTION-
INDUCED LATERAL SPREADING AND HISTORIC LATERAL SPREADING,
NORTHERN DIXIE VALLEY, NEVADA**

Principal Investigators / Authors:

S. John Caskey, Department of Geosciences, San Francisco State University, San Francisco, CA 94132; phone: 415-405-0353; fax: 415-338-7705; e-mail: caskey@sfsu.edu

Robert J. Watters, Department of Geological Sciences and Engineering, University of Nevada, MS 172, Reno 89557; e-mail: watters@mines.unr.edu

Program Element: III

Research supported by U.S. Geological Survey (USGS) Department of the Interior, under USGS award number 06HQGR0067. The views and conclusions contained in this document are those of the authors and should not be interpreted as necessarily representing the official policies, either expressed or implied, of the U. S. Government.

AWARD# 06HQGR0067

TITLE: INVESTIGATION OF LARGE MAGNITUDE PALEOLIQUEFACTION-INDUCED LATERAL SPREADING AND HISTORIC LATERAL SPREADING, NORTHERN DIXIE VALLEY, NEVADA

Principal Investigators / Authors:

S. John Caskey, Department of Geosciences, San Francisco State University, San Francisco, CA 94132; phone: 415-405-0353; fax: 415-338-7705; e-mail: caskey@sfsu.edu

Robert J. Watters, Department of Geological Sciences and Engineering, University of Nevada, MS 172, Reno 89557; e-mail: watters@mines.unr.edu

TECHNICAL ABSTRACT

The primary objectives of our investigation were to: 1) complete the mapping and compilation of the distribution of the late Holocene fault scarps along the eastern escarpment of the Stillwater Range and related liquefaction-induced lateral spread structures in the fan piedmont area; 2) structurally analyze areas of intensive liquefaction induced deformation to estimate lateral spread displacements; and 3) to conduct site specific drilling investigations using both Standard-Penetration and Cone-Penetration tests (SPT and CPT) as complimentary aids in providing constraints on the subsurface geometry and characteristics of the liquefiable layer(s). Our limited structural analyses together with structural relations in areas not yet analyzed in detail indicate that lateral-spread displacements we observe in Dixie Valley are far greater than those documented in case histories worldwide, and further indicate that a complex set of factors are responsible for such large-magnitude lateral spreading. Our drilling and geotechnical analyses identified that the deposits are non-uniform in nature and include clays interfingered with silts, sands and gravels. The deposits under seismic loading effects can fail by liquefaction of sand, and cyclic failure and translational shear within the clay. Our preliminary interpretation is that the late Holocene lateral spreading initiated by seismically-induced liquefaction of sand and that continued lateral spread displacement along the sloping fan piedmont areas was facilitated by translational shear failure within clay layers.

The study documents both geologic and geotechnical aspects of perhaps the most extreme, well-preserved case of paleoliqefaction in the Basin and Range in an area where lateral spreads formed along very gently sloping ground in the absence of a free face. Documentation of the extreme lateral spreading in Dixie Valley provides an important analogue for potentially reducing losses associated with liquefaction hazards in more populated areas of the Basin and Range, such as Salt Lake City, Las Vegas, and the Reno-Carson City regions where similar geologic conditions may exist.

FINAL TECHNICAL REPORT—

INVESTIGATION OF LARGE-MAGNITUDE PALEO-LIQUEFACTION-INDUCED LATERAL SPREADING, NORTHERN DIXIE VALLEY, NEVADA

INTRODUCTION

The primary objectives of our investigation were to: 1) complete the mapping and compilation of the distribution of the late Holocene fault scarps along the eastern escarpment of the Stillwater Range and related liquefaction-induced lateral spread structures in the fan piedmont area; 2) structurally analyze areas of intensive liquefaction induced deformation to estimate lateral spread displacements; and 3) to conduct site specific drilling investigations using both Standard-Penetration and Cone-Penetration tests (SPT and CPT) as complimentary aids in providing important constraints on the subsurface geometry and characteristics of the liquefiable layer(s).

In this report we summarize the geological and geotechnical results of our study. Detailed maps of the late Holocene earthquake ruptures along the eastern escarpment of the Stillwater Range (i.e., the Dixie Valley fault) and lateral-spreads and related structures in the fan piedmont areas and along the playa margin are included as Appendices 1A-G.

METHODS

Field mapping of late Holocene fault scarps and liquefaction-induced lateral spreads (Figure 1) were conducted in the field on 1:12,000-scale low-sun-angle photos and then compiled on 1:24,000-scale topographic base maps (Appendices 1A-G). We conducted structural analyses of the lateral spreading and compressed lacustrine strata near Dixie Comstock (Figures 2 and 3). The paleoliquefaction-related features are very well-preserved and a detailed total station profile and a structural cross section across the compressed lacustrine sediments along the playa margin form the basis for estimating lateral spread displacements near Dixie Comstock. Similar detailed structural analyses of lateral spread displacements in the area of Dixie Meadows (Figure 1) are currently in progress.

Our drill studies employed both Standard Penetration Test (SPT) and the Cone Penetration Test (CPT) as aids in identifying potential liquefiable layers. In addition to performing both types of tests (as they are complimentary), our analyses were also augmented by shear wave velocity data collected during CPT drilling which permitted further analyses and aid in our assessments of liquefaction potential. SPT data was collected for 6 out of 8 total drill locations (N-1, N-3, M-4, M-6, S-7 and S-8; Figure 1, Appendices 1C and 1D). CPT data was collected for 7 of the 8 drill locations (N-2, N-3, M-4, M-5, M-6, S-7, and S-8; Figure 1, Appendices 1C and 1D). Only analyses for our northernmost drilling profile (N-1, N-2, and N-3) are completed and discussed in this report.

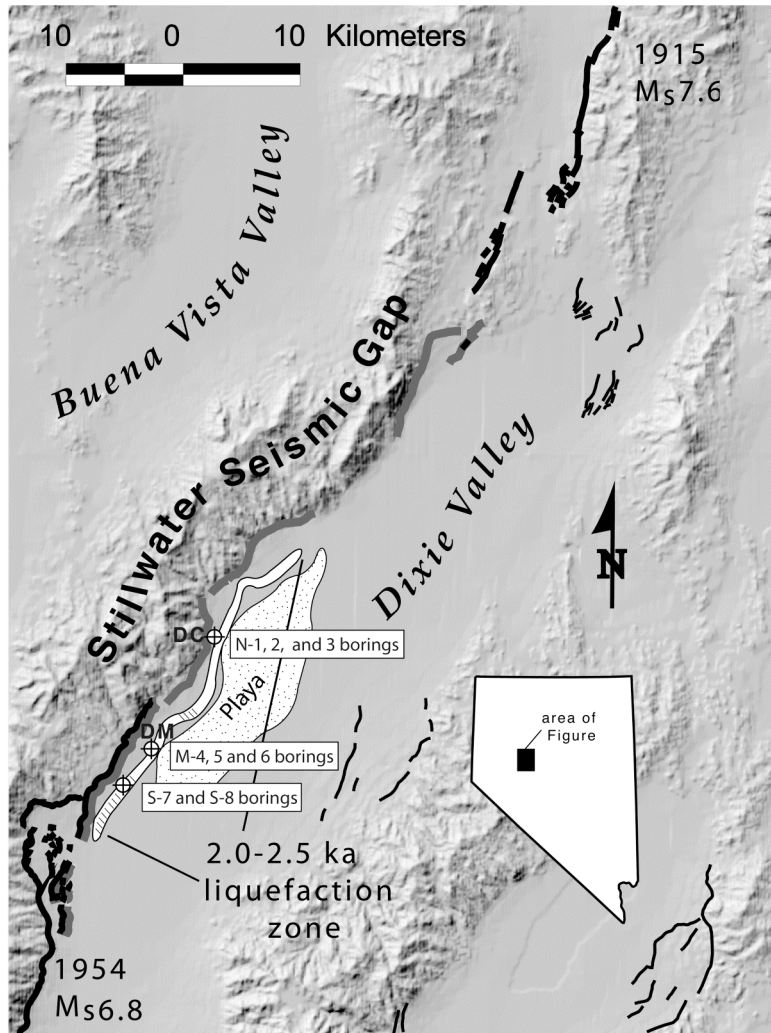


Figure 1. Location map showing historic rupture zones (black) of the 1954 Dixie Valley and 1915 Pleasant Valley earthquakes, the rupture zone of the 2.0-2.5 ka penultimate earthquake in the southern part of the Stillwater Gap which overlaps with the 1954 rupture zone (thick gray line), and the approximate zone of liquefaction-induced lateral spreads associated with the penultimate event. Hatched areas within the 2.0-2.5 ka liquefaction zone represent areas where 1954 lateral spreads also occurred (Slemmons, 1957; Caskey et al., 1996). Squares indicate locations referred to in the text: DC - Dixie Comstock; DM - Dixie Meadows; TC - Terrace Creek. Approximate locations for the eight boreholes (N-1, 2, and 3; M-4, 5, and 6; and S-7 and 8) are shown. Accurate locations for each of these drill holes are shown in Appendices 1C and 1D).

RESULTS

Constraints on amount of lateral spread displacement near Dixie Comstock

The “compressed zones” along the playa margin (Figures 2, 3, and 4; Appendices 1C, 1D) are interpreted as being caused from the basinward-directed, lateral-spread displacements along the gently sloping areas along the outer fan piedmont. This interpretation follows from the observation that the compressed zones are found only in areas that are down-slope from the most intense zones of lateral spreading.

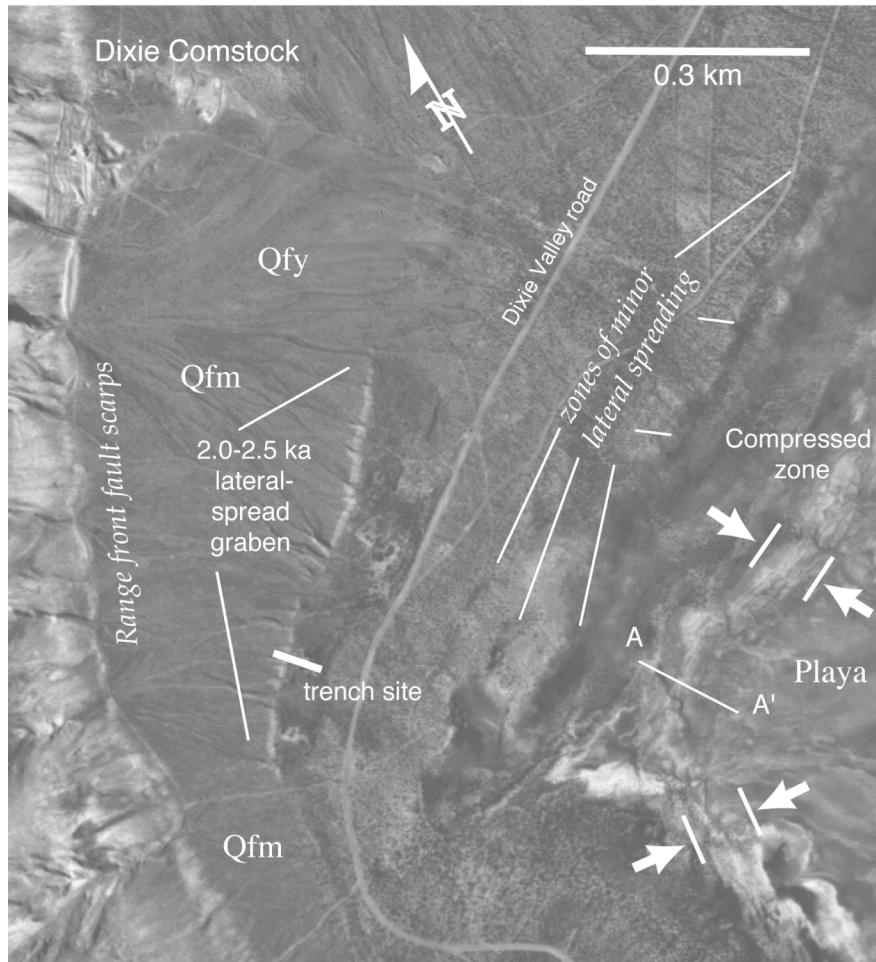


Figure 2. Low-sun-angle photo of the Dixie Comstock area showing the 2.0-2.5 ka range-front fault scarps, lateral-spread graben, other minor lateral-spread zones, and the compressed zone along the playa margin. Also shown are the locations of the trench and cross section A-A' across the compressed zone (Figure 3).

At Dixie Comstock (Figures 1 and 2; Appendix 1C) the compressed zone is not as broad as it is southeast of Dixie Meadows (Figures 1 and 4; Appendices 1C and 1D). However, near Dixie Comstock the lacustrine strata are severely buckled up along folds and imbricate “thrusts” that parallel the edge of the playa across a width of ~100 m. (*For comparison, the width of the compressed zone near Dixie Meadows is over 500 m*). Cleaned-off exposures across the 100 m compressed zone near Dixie Comstock revealed 14 different exposures of deformed and repeated Mazama tephra (6.9 ka) (e.g., Figure 3). The ash bed, at most locations, dips to the east indicating that the strata are repeated mostly along multiple west-vergent “thrusts” and overturned folds. The ash bed is ubiquitously overlain by a 10-15 cm-thick, halite-“cemented” layer that has apparently given rigidity to the lake sediments and allowed for the development of the somewhat regular “fold and thrust belt” geometry of the compressed zone. Bedding attitudes at each of the 14 tephra exposures, a total station profile accurately marking each exposure location, and a hand dug pit that revealed the depth to the Mazama ash east of the deformed zone provided constraints for a detailed, reconstructable cross section along the transect (Figure 3). Most importantly, the well-defined, fully-exposed stratigraphy and

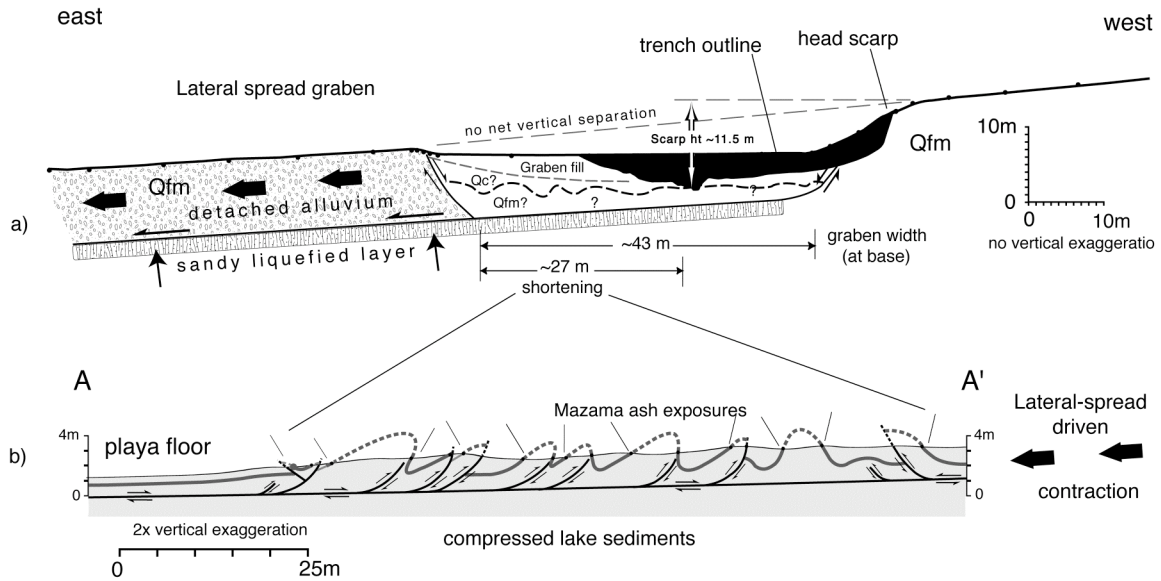


Figure 3. a) Conceptual cross section across the lateral-spread graben south of Dixie Comstock. b) Cross section A-A' across the playa-margin compressed zone located down-slope from the lateral spread graben in a) (see Figure 2 for location). Cross section is constrained from attitudes of 14 repeated beds of 6.9 ka Mazama ash exposed across the zone of folded and thrust-imbricated lacustrine sediments and a test pit excavated into the playa floor east of the disrupted zone (note east is to the left). The deformed beds are interpreted to be the result of contractional accommodation of the down-slope movement of relatively cohesive Qfm fan deposits above a liquefied zone of water-saturated lacustrine sand. Cross section A-A' suggests approximately 27 meters of shortening across the zone. (Note that shortening was calculated from a non-vertically exaggerated version of the cross section). The graben width is about 43 meters, suggesting that much of that width represents actual down-slope movement of the detached alluvium east of the graben. Note that both figures are shown at the same horizontal scale. The two cross sections are separated by a down-slope distance of about 300 m.

structure together with the rigid nature of the contracted lake deposits allows for viable estimates of shortening across the deformed zone, which in turn, must reflect the amount of lateral-spread displacement up-slope of the playa margin.

The cross section (Figure 3b) suggests about 27 m of shortening across the compressed zone at this location. It stands to reason that the amount of shortening across the compressed zone should approximately balance with the amount of horizontal lateral-spread displacement upslope from the playa. Although lateral spreads formed across the entire area between the playa margin and the large graben at the trench site, the greatest spreading probably occurred across the largest graben. At the trench site, the graben width is ~43 m. The 27 m of shortening across the playa margin suggests that a significant portion of the graben width was produced by lateral-spread displacement. At present we can only speculate that the amount of lateral spreading near Dixie Meadows (Figures 1 and 4; Appendix 1D) represented by the extreme contraction of playa-margin sediments in this area is far greater than the estimated lateral spread displacement of ~27 m near Dixie Comstock. The large lateral spread displacements we observe in Dixie Valley (>27 m) are far greater than maximum measured horizontal displacements recently compiled for 45 lateral spread case histories (Faris et al., 2006), which reach a maximum of less than 7 m (Figure 5). The much larger lateral spread displacements we observe in Dixie Valley suggest that a complex set of geotechnical factors are responsible for such large-magnitude lateral spreading.

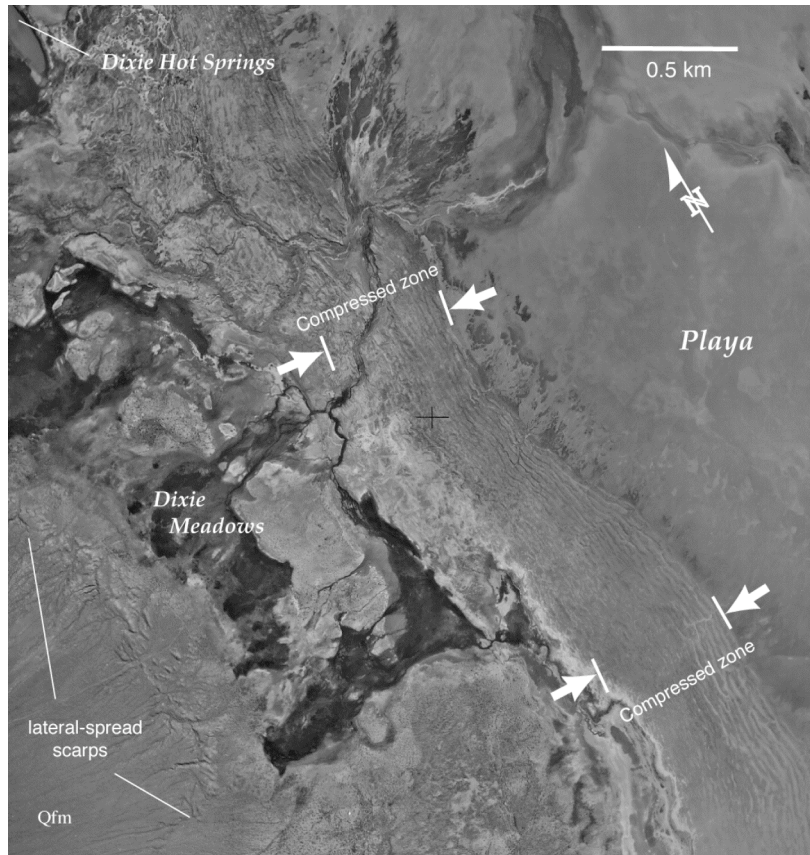


Figure 4. Low-sun-angle photo for the area of Dixie Meadows (Figure 1) showing 2.0-2.5 ka lateral spreads and compressed lacustrine strata along the playa margin.

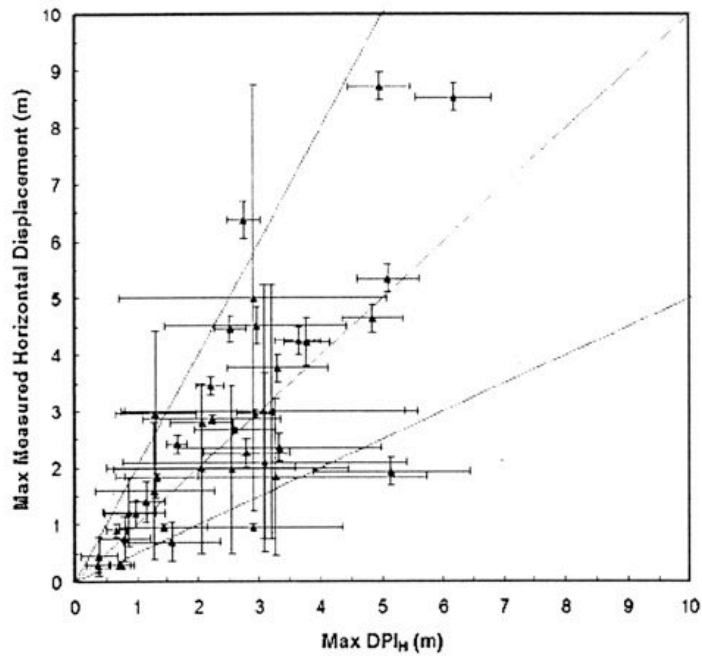


Figure 5. Comparison of maximum Displacement Potential Index (x-axis) versus maximum measured horizontal lateral spread displacements (y-axis) for 45 case histories of lateral spreading (from Faris et al., 2006).

Geotechnical Overview

The purpose of the geotechnical investigation within our proposal was to establish the soil characterization and soil strength, and their relationship to the distribution, failure modes, and morphology of seismically induced lateral spreads within Dixie Valley. Preliminary data analysis and calculations show that we have been successful in this goal, though as a result of subsurface complexity and limited funds only the northern part of the lateral spreading has been analyzed.

Our drilling and analyses identified that the deposits are non-uniform in nature and include clays interfingered with silts, sands and gravels. The deposits under seismic loading effects can fail by liquefaction of sand, and cyclic failure and translational shear within the clay. Successful site characterization required a substantial number of samples from different parts of the deposit for characterization. Consequently only the northern most part of the extensive lateral spread has been assessed.

Geotechnical investigations

Three sites were drilled on the edge of the playa at locations where lateral spreading had previously been identified. The boring locations are situated east of the Stillwater Range front fault system. The subsurface was interpreted to be composed of alluvial fan material washed down from the westward bounding Stillwater Range and beach gravel, sands and fines from the eastward bounding pluvial Lake Dixie. The most promising site for the subsurface investigation was the most northerly site where an earlier trench had been excavated at the head scarp of the lateral spread. A profile overview of the northernmost site is given in Figure 6. The trench had permitted age dates to be assigned on the lateral spread event though the trench did not intersect a failure surface on which the lateral spread had developed. Given the uncertainty of the depth of the failure surface the first drill site locations were selected so that potential suitable failure horizons could be identified and a cross section developed for the northern site. Extensive laboratory testing, liquefaction and stability analyses have been performed from data obtained from the northern site. Two other sites, located farther south were investigated, a middle and southern site, and a limited amount of drilling carried out where lateral spreading features had similarly been identified from aerial photography and morphology. Neither of these sites has been analyzed as a consequence of a shortage in funds, though soil samples were collected permitting subsurface lithology to be determined together with Standard Penetration Testing (SPT) and Cone Penetration Testing (CPT) data. The middle and southern sites will be analyzed when funds become available.

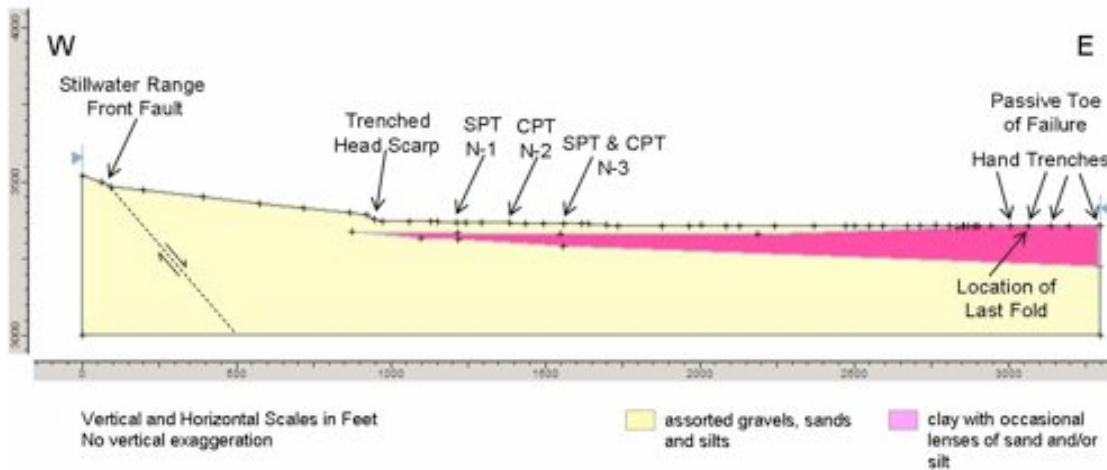


Figure 6. Overview of north site showing slope profile and boring locations.

Results from the Northern Site (borings N1, N2, N3)

The site investigation and associated borings were carried out during August 2006 employing Gregg Drilling mobilized from their Martinez, California office. An auger drilling rig capable of Standard Penetration Testing (SPT) work and a Cone Penetration Testing (CPT) rig with a seismic cone were utilized and provided interesting results for the northernmost site. Drilling consisted of hollow stem augured borings with undisturbed sample collection on 2.5 foot centers and continuous CPT testing with seismic CPT on 5 foot centers. A total of 170 feet (52 meters) of hollow stem drilling combined with SPT and an equal amount of undisturbed sampling and continuous CPT and seismic CPT at 5 foot intervals was performed (Figure 7). Figure 7 details results from the CPT profiling of the subsurface conditions plotted against depth and includes cone bearing pressure (tsf), sleeve friction (tsf), and shear velocity (ft/sec). The soil lithology log interpretation is based on correlations by Robertson (1990) and differed significantly from tube samples obtained from SPT sampling particularly in recognizing clay rich soils which were interpretive as silt from the CPT profiling. At the edge of the playa where weak ground surface conditions did not permit mechanized drilling hand, auguring to depths of 15 feet (4.5 meters) with shear vane testing were conducted.

The subsurface borings showed that the anticipated and somewhat simple subsurface picture of an alternating silt and sand sequence was complicated by thick horizons of weak clays overlain by unconsolidated sediments.

At the edges of the playa where the hand auguring was performed the clay sequence progressively changed from a tan color nearest the ground surface to green at a deeper depth, then to blue and finally black clay at the deepest extent augured. No discernible relationship between strength and color was determined from laboratory and in-situ shear testing. The analyses of subsurface samples by XRD techniques identified that the black low-strength clay consisted primary of smectite. The clay quickly formed a

beige oxidized rind on exposure to air which initially was thought to be organic but total organic carbon (TOC) analysis indicates that it contains less than 1% organic material.

The preliminary field work indicated the presence of sand boils and fissures consistent with seismically induced lateral spreading as a result of liquefaction however the low-strength clay identified from the sub-surface investigation and analyses presents the possibility of seismically-induced lateral spreading from cyclic failure. The clay horizons were analyzed for cyclic failure and also appraised given their low shear strength as providing a potential translational shear failure surface for block failure.

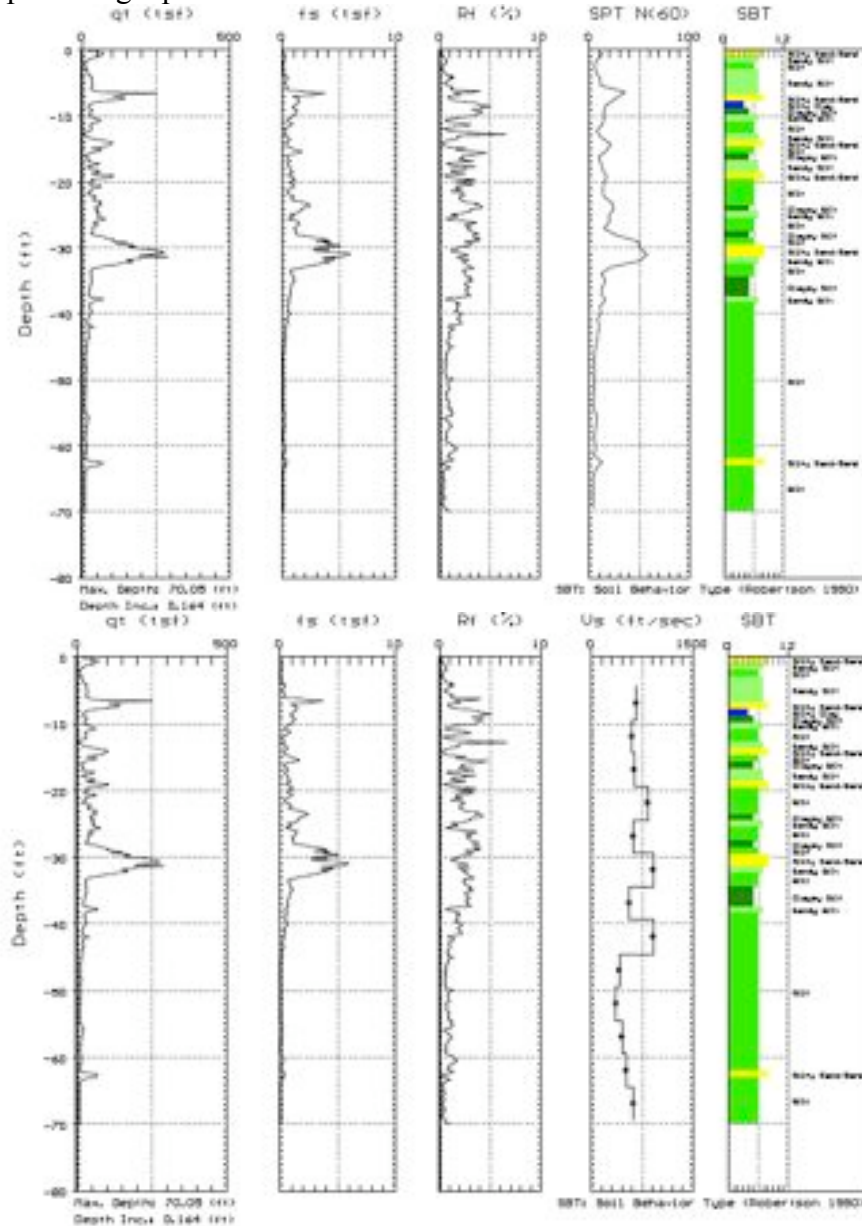


Figure 7. Typical logs from CPT boring number CPT - 03A.

Laboratory testing

Soil analysis tests including unit weight, Atterberg Limits, particle size distribution, undrained direct shear strength (Su), x-ray diffraction and organic content

were conducted on the soil samples obtained from undisturbed sampling from borings and auguring. Table 1 details the type and number of tests conducted on the samples.

Table 1. Number and type of soil analyses from the northern site.

Boring no.	Unit Weight	Atterberg Limits	Gradation Analyses	Direct Shear	XRD	TOC
N - 1	14	14	24	4	1	1
N - 3	43	18	17	12	2	2
Auger	1	5		1 + 5 vane	3	3

Figures 8 and 9 show typical gradation curves for both material types – granular silty sands and clay. Further analyses were performed on the clays to establish plasticity characteristics (LL and PI) of the underlying clays, borings N1 and N3, and also for the hand dug trenches and augured borings in the playa (Figures 10, 11, and 12).

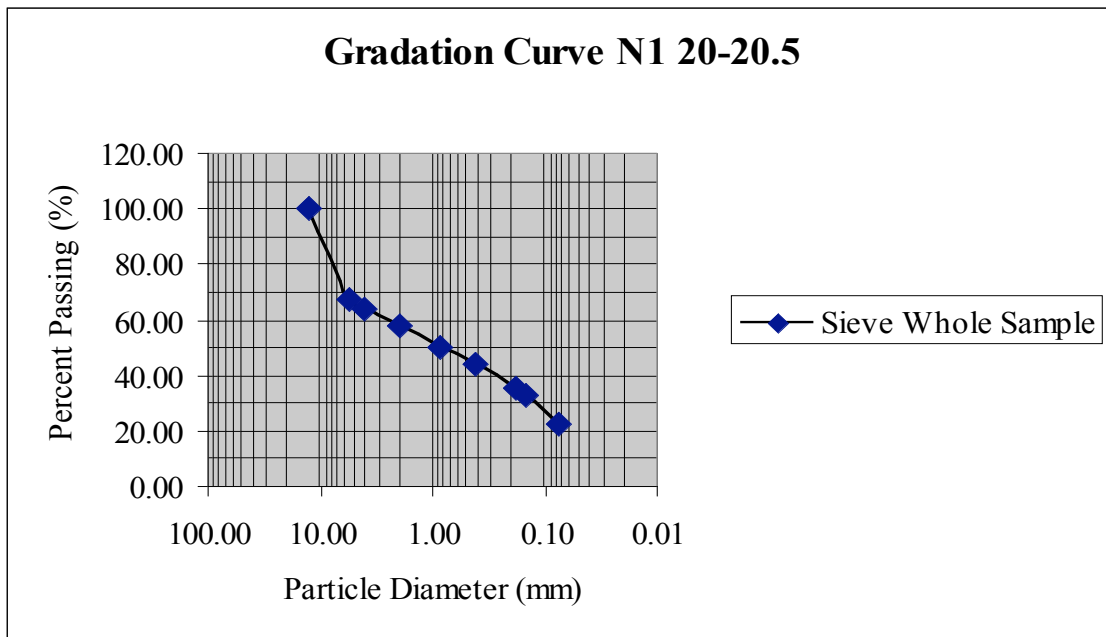


Figure 8. Typical gradation curve for granular material classification SM or SC - silty or clayey sand with gravel.

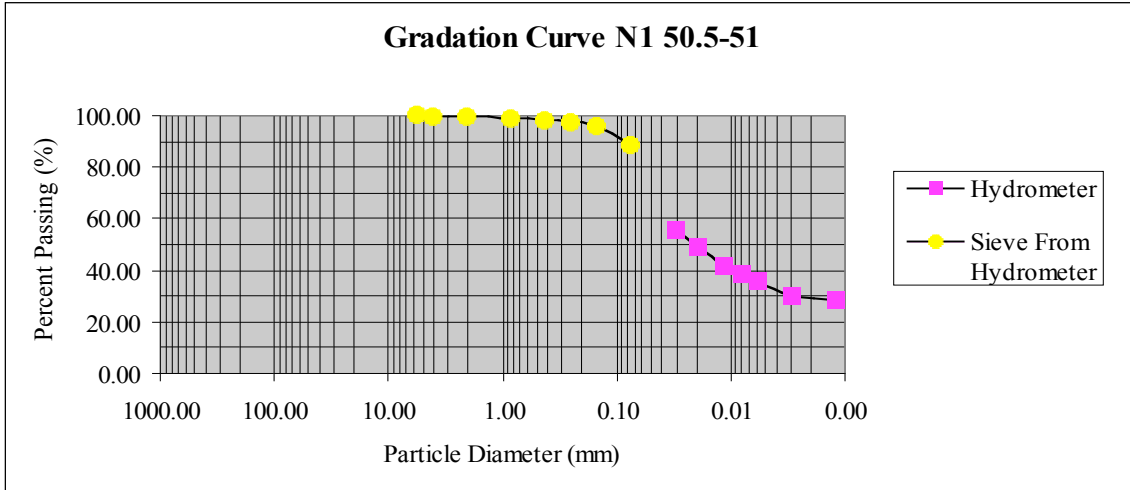


Figure 9. Typical gradation curve for underlying clay, classification CH - fat clay.

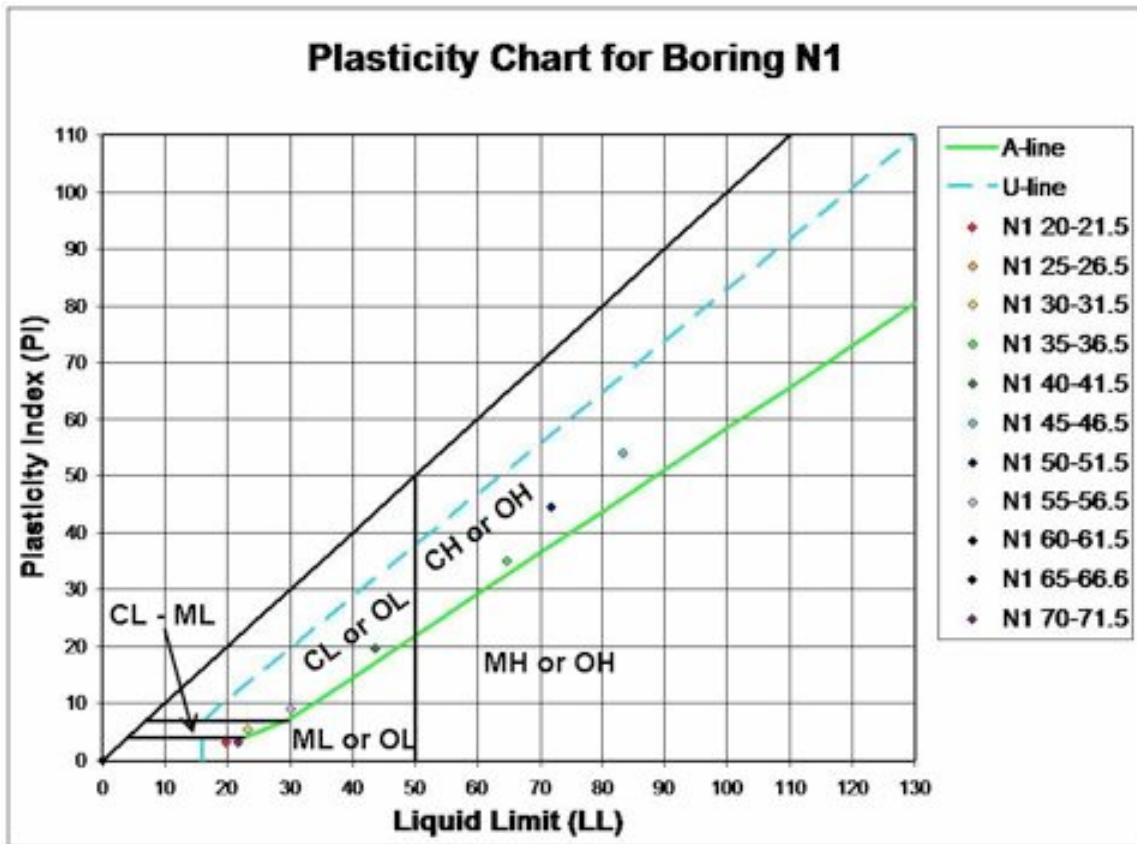


Figure 10. Results for boring N1 – plasticity indices.

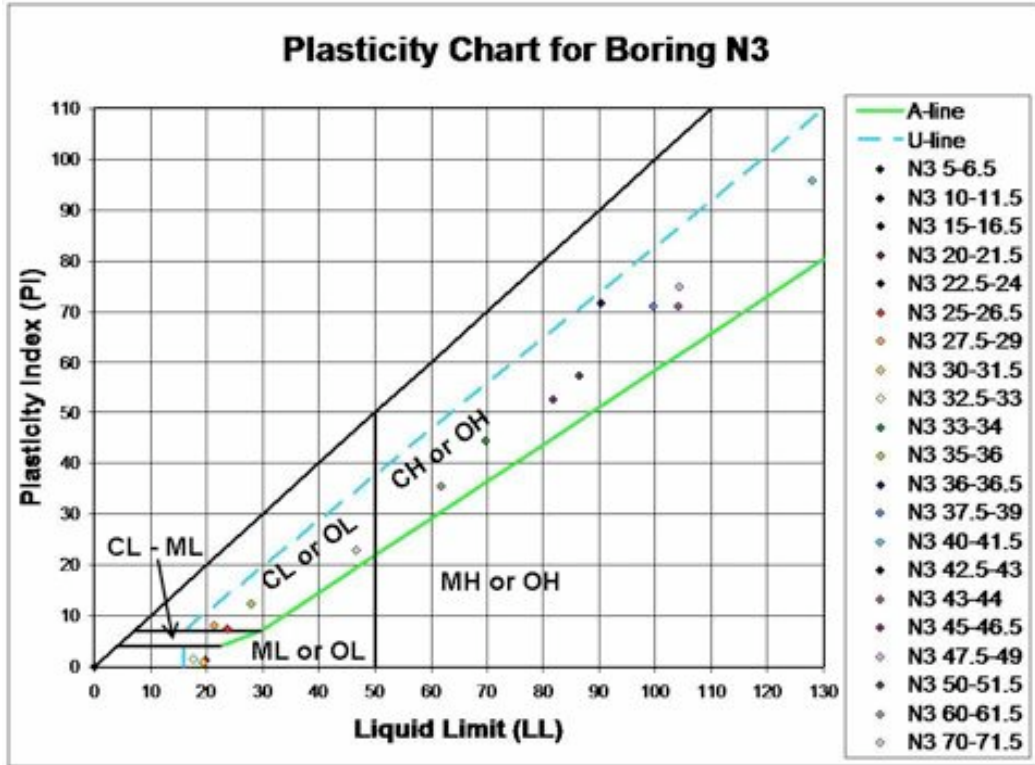


Figure 11. Results for boring N3 – plasticity indices.

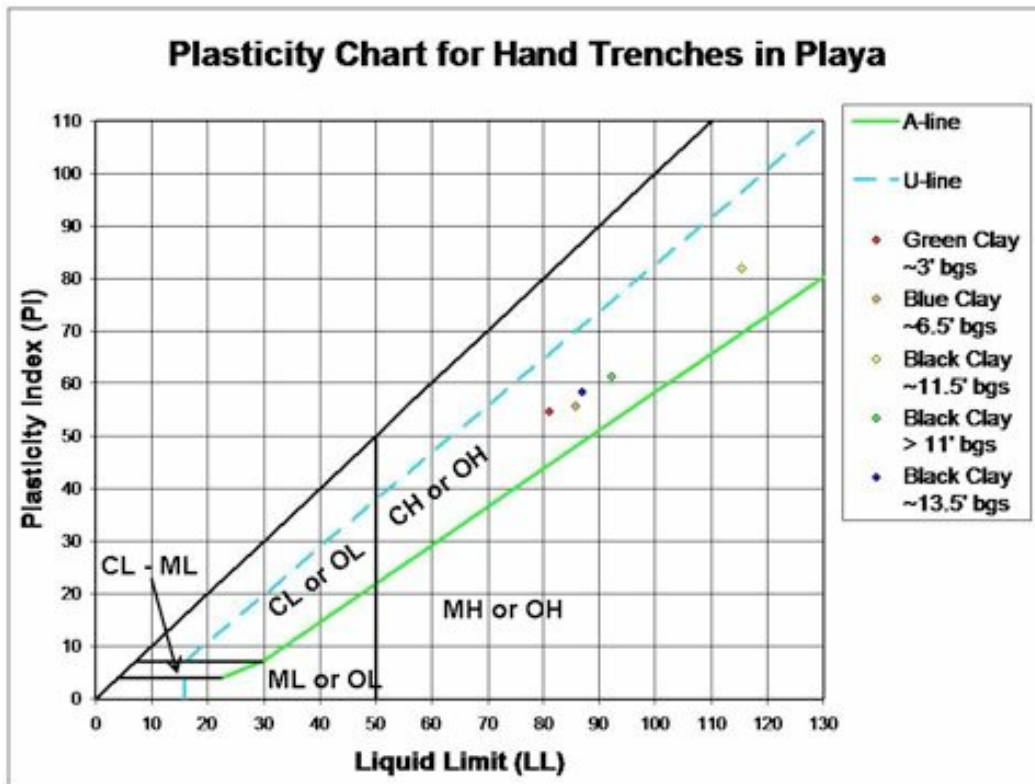


Figure 12. Results for hand trenches – plasticity indices.

The anticipated subsurface stratigraphy did not include clays as part of a liquefaction analysis. For this reason, standard clay samplers such as Shelby tubes were not ordered for the subsurface investigation. The clay samples used for testing were obtained from SPT split spoons or from hand augers and are considered disturbed samples in common practice. These samples are regarded as marginally remolded in preparation for direct shear tests and the S_u values obtained are expected to be lower than the undisturbed peak values. Shear vane analyses performed in the playa provided some constraint on undisturbed S_u values.

Clay strengths were found to vary with normal load and moisture content which is atypical of most clays but a potential difficulty with swelling clays, such as smectites, which can hold greater than 100% moisture. As testing proceeded, some clays did not have adequate permeability to become saturated during the allotted testing time. Due to this variation of strength with normal load, clay strengths were treated as dependent on friction and cohesion and expressed as Mohr-Coulomb materials in the appropriate analyses.

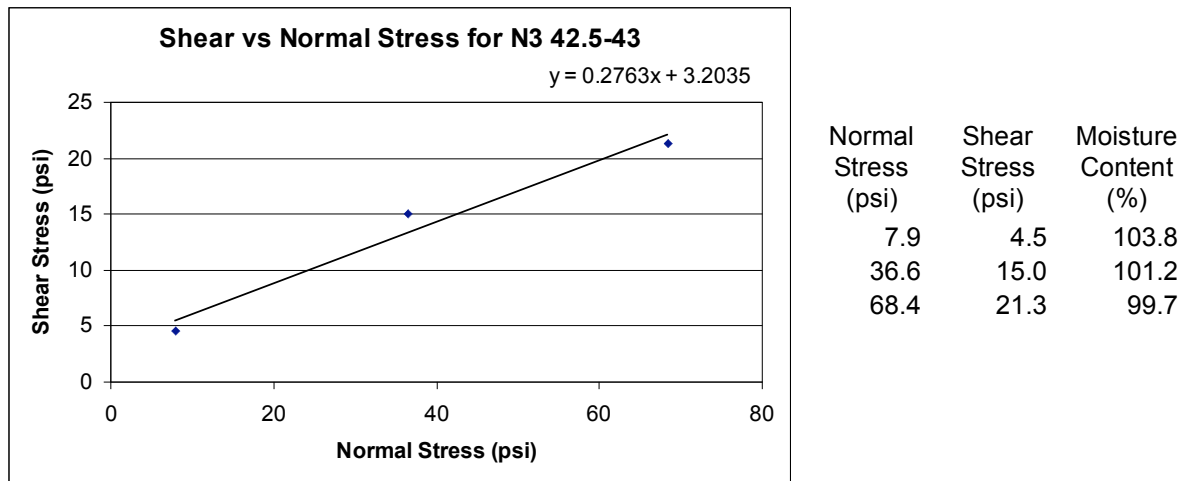


Figure 13. Typical shear stress versus normal stress plot from clay direct shear testing. Chart to right shows moisture content as measured from the failure surface for each test.

Liquefaction, cyclic failure or translational shear failure

The results from the in situ and laboratory testing suggest that the sand, silt, and clay horizons can experience failure given the strength and gradation values found by either liquefaction or cyclic failure from earthquake loading. Both mechanisms result in strength loss and deformation from the cyclic nature of earthquake loading and the slow dissipation of pore water pressure causing an increase in fluid pressure by multiple loading cycles. However, the characteristics and procedures for measuring the strengths of cohesionless soils (sands) and cohesive soils (clays) are very different and for this reason their liquefaction potentials must be assessed differently.

The liquefaction and cyclic failure theory used in these analyses has been in development since 1982 by various researchers (Boulton, Seed, and Idriss (1982), Seed, Cetin et al (2003), and Boulanger, Idriss, (2006). Peak ground accelerations were

calculated following the research by Campbell and Bozorgnia (2007). The RocScience program Slide, version 5.0, was used for sliding block analyses. Preliminary findings are detailed below in Figures 14 through 18.

The plasticity index (PI) of the soil was used for determining the appropriateness of whether a sample was analyzed for liquefaction or cyclic failure. The boundary of $PI = 7$ was used as the dividing line with soils having a $PI < 7$ analyzed for liquefaction and soils with a $PI > 7$ analyzed for cyclic failure. Soils close to a $PI = 7$ were analyzed for both failure modes. Once the appropriate soil parameters of PI, fines content (% fines), unit weight, and undrained shear strength (S_u) had been found for lithologies at different depths the potential for different failure modes was calculated.

Factor of safety results for soil depths, soil types, and failure modes

The site cross-section is contained in Figure 14 detailing the depth and types of soils encountered in boreholes N1, N2 and N3. Factor of safety calculations for the stability of the different soils at different depths below the ground surface under similar peak ground accelerations (pga) are detailed in Figures 15 through 18. The calculations are specifically for the soils encountered in all three boreholes for the northern site (N1, N2, and N3). The type of analyses performed (SPT and CPT liquefaction, and CPT cyclic failure) and resulting factor of safety are annotated on each figure.

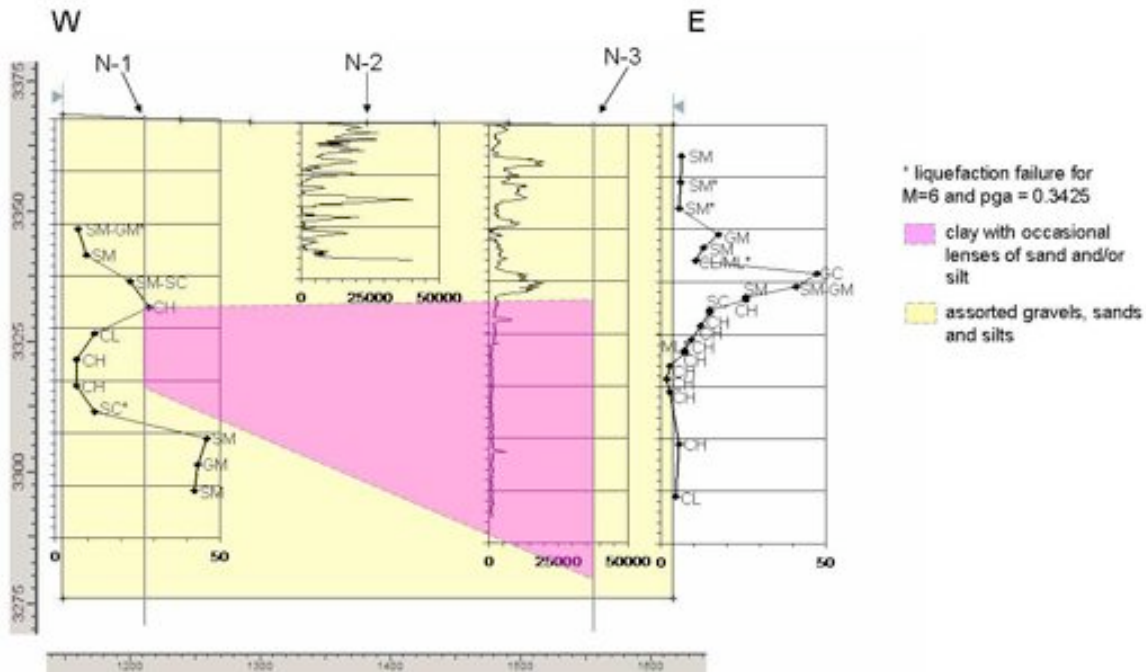


Figure 14. Cross-section showing subsurface results from drilling investigation. Vertical and horizontal scales are in feet; vertical exaggeration is approximately 4 times.

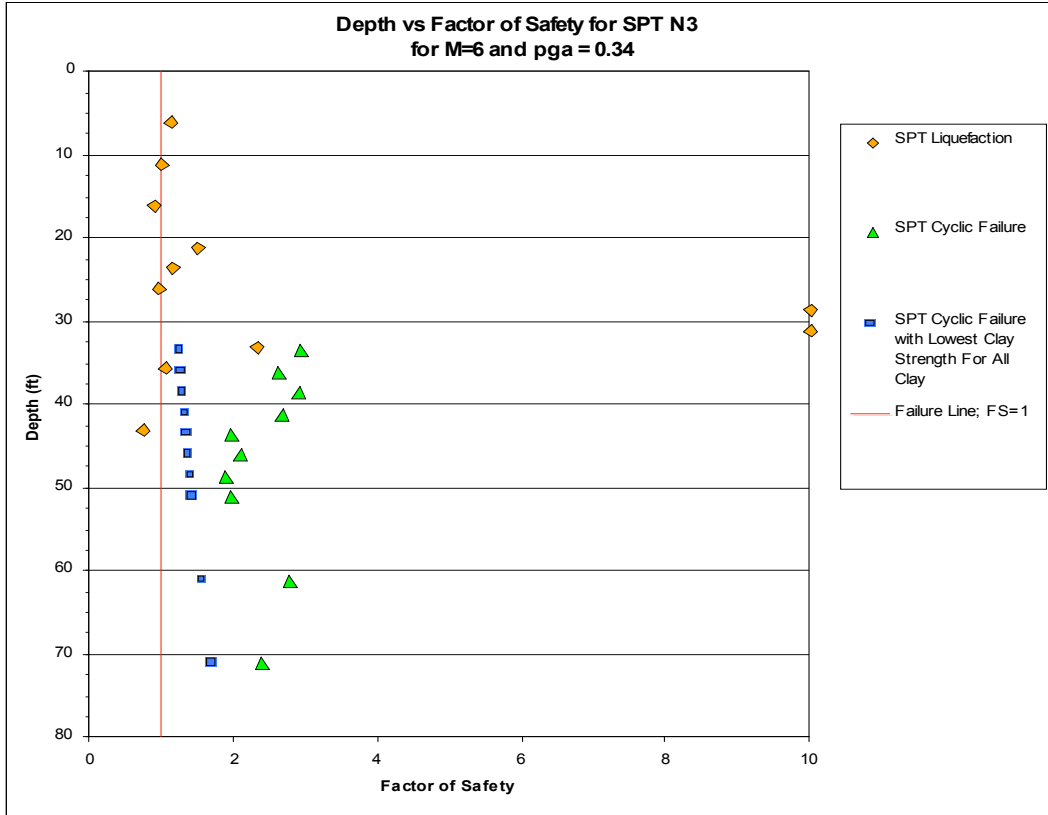


Figure 17. Factor of safety results for SPT data from borehole N3.

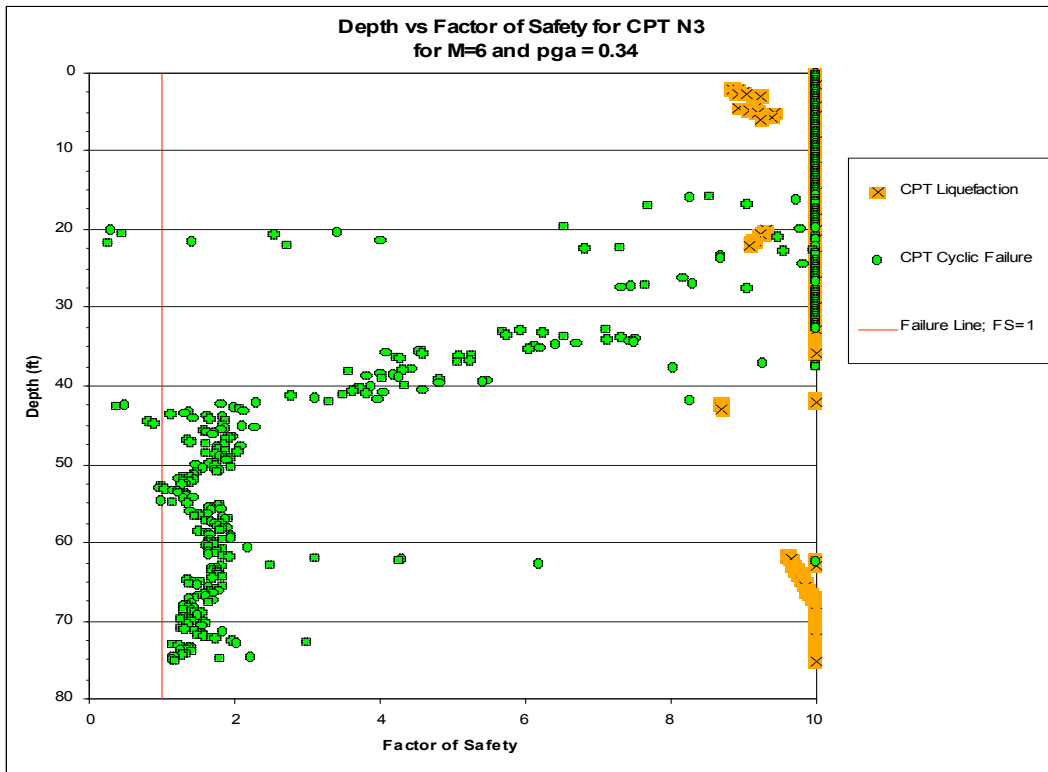


Figure 18. Factor of safety results from CPT data from borehole N3.

Figure 18 contains a typical factor of safety result from a translational failure stability analysis (Janbu analysis). This type of failure mode was assessed given the low shear strength determined for the clay.

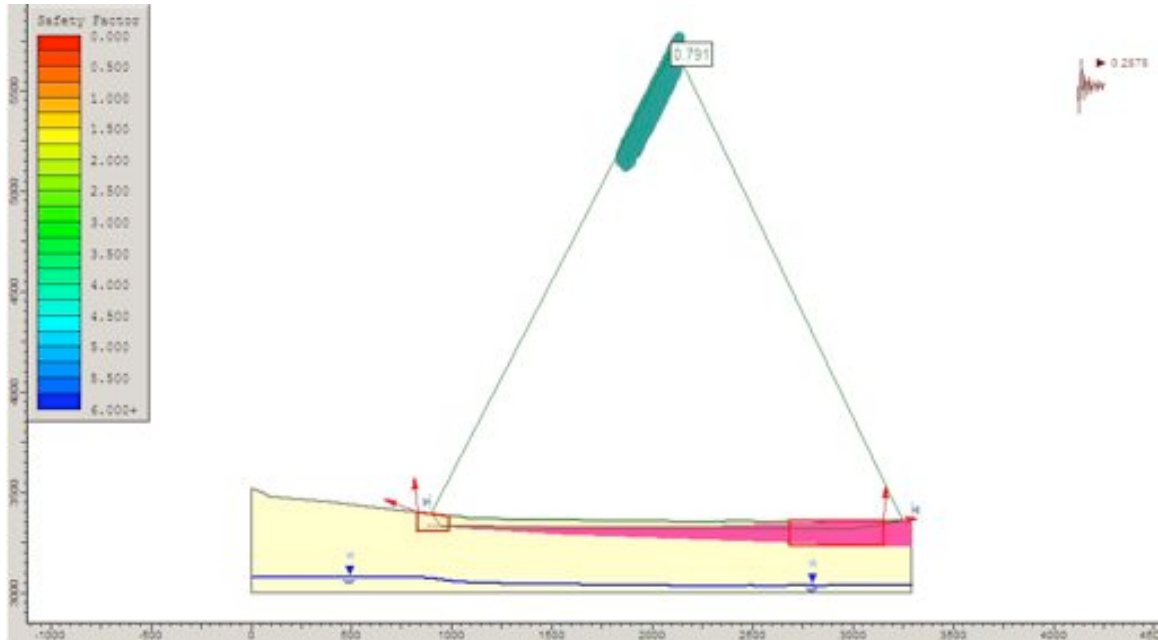


Figure 19. Results from noncircular failure analysis showing a factor of safety of 0.79 with an applied peak ground acceleration of 0.28.

PRELIMINARY CONCLUSIONS

Lateral spreading from the destabilizing influence of seismic loading has been confirmed from analyses of subsurface stratigraphy, borings, laboratory and in-situ strength testing, and from stability calculations.

Using a limit equilibrium analysis of increasing earthquake magnitude and peak ground acceleration, the first horizons predicted to fail were for a magnitude 6.0 event with a peak ground acceleration of 0.34. Preliminary liquefaction analyses of penetration and soil data from SPT borings from the northernmost site indicated that the weakest horizon is located approximately between 20 to 25 feet below the ground surface. This horizon has a fines content of about 3% and a PI of 3. Intermittent layers at greater depths, interpreted as sand lenses, were also found to be weak, but were not found to be continuous between the borings.

Preliminary CPT cyclic failure analyses indicated that weak horizons were also present at approximately 20 feet below ground surface. However, clays were not found to be present at this depth in the SPT boring logs so cyclic failure at these depths is unlikely. CPT cyclic failure analyses also indicated a weak horizon at approximately 42.5 feet below ground surface in boring N3. This horizon is near the upper limit of the clay thickness identified in SPT samples.

Preliminary translational block failure analyses indicated that a noncircular sliding block failure through the clay is possible. This failure was predicted to occur for a magnitude 5.5 earthquake event with a peak ground acceleration of 0.28. While initially this appears to be the critical failure mode, it should be noted that the sliding block model is not nearly as detailed as the liquefaction and cyclic failure analyses and clay strengths were generalized.

References:

Boulanger, R. M. and Idriss, I.M. (2006). Liquefaction susceptibility for silts and clays, Jour. Geot. Geoenv. Eng., ASCE, pp. 1413-1426.

Campbell, K. W, and Bozorgnia, Y, (2007). NGA Ground Motion Relations for the Geometric Mean Horizontal Component of Peak and Spectral Ground Motion Parameters, Pacific Earthquake Engineering Research Center, University of California, Berkeley, p. 240.

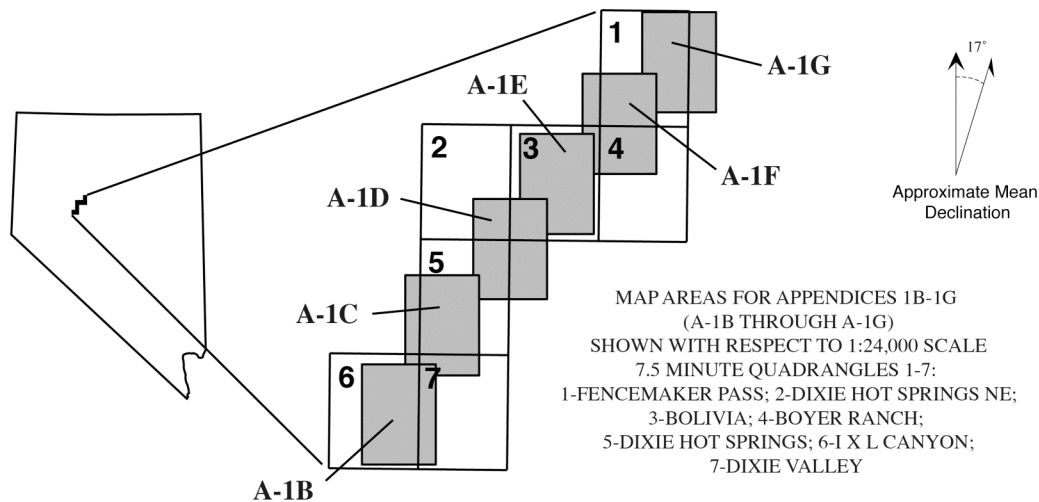
Boulton, H., Seed, R.B, and Idriss, I.M, (1982) Ground motions and soil liquefaction during earthquakes, EERI, Berkley, California, p.134.

Faris, A.T., Seed, R.B., Kayen, R.E., Wu. J. (2006). A semi-empirical model for the estimation of maximum horizonatal displacement due to liquefaction-induced lateral spreading, 8th U.S. National Conference on Earthquake Engineering, Earthquake Engineering Research Institute (EERI).

Robertson, P.K., (1990), Soil classification using the Cone Penetration Test, Canadian Geotechnical Journal, vol. 27, pp.151 -158.

Seed, R.B., Cetin K.O, Moss R.E.S. Kammerer A.M., Wu J. Pestana, J.M, Riemer, M.F. Sancio R.B, Bray J.D, Kayen, R.E, Faris, (2003).Recent advances in soil liquefaction: a unified and consistent framework: Report number EERC 2003-06, p. 71.

APPENDIX 1A. MAP EXPLANATION FOR APPENDICES 1B-1G. FAULT RUPTURES AND SECONDARY, LIQUEFACTION-INDUCED FEATURES ASSOCIATED WITH HISTORIC AND LATE HOLOCENE EARTHQUAKE FAULTING IN THE STILLWATER SEISMIC GAP, DIXIE VALLEY, NEVADA



EXPLANATION OF SYMBOLS

- 

Fault scarp formed in 1954 (red); Fault scarp in alluvial deposits (black), unless otherwise noted on map - Bar and ball on downthrown side.
- 

Compound fault scarp (CS) showing 1954 displacements - Bar and ball on downthrown side. Most of these fault scarps also exhibit youthful displacements that occurred during the ~2.5 ka fault rupture of the Stillwater Gap (i.e., the "Gap event").
- 

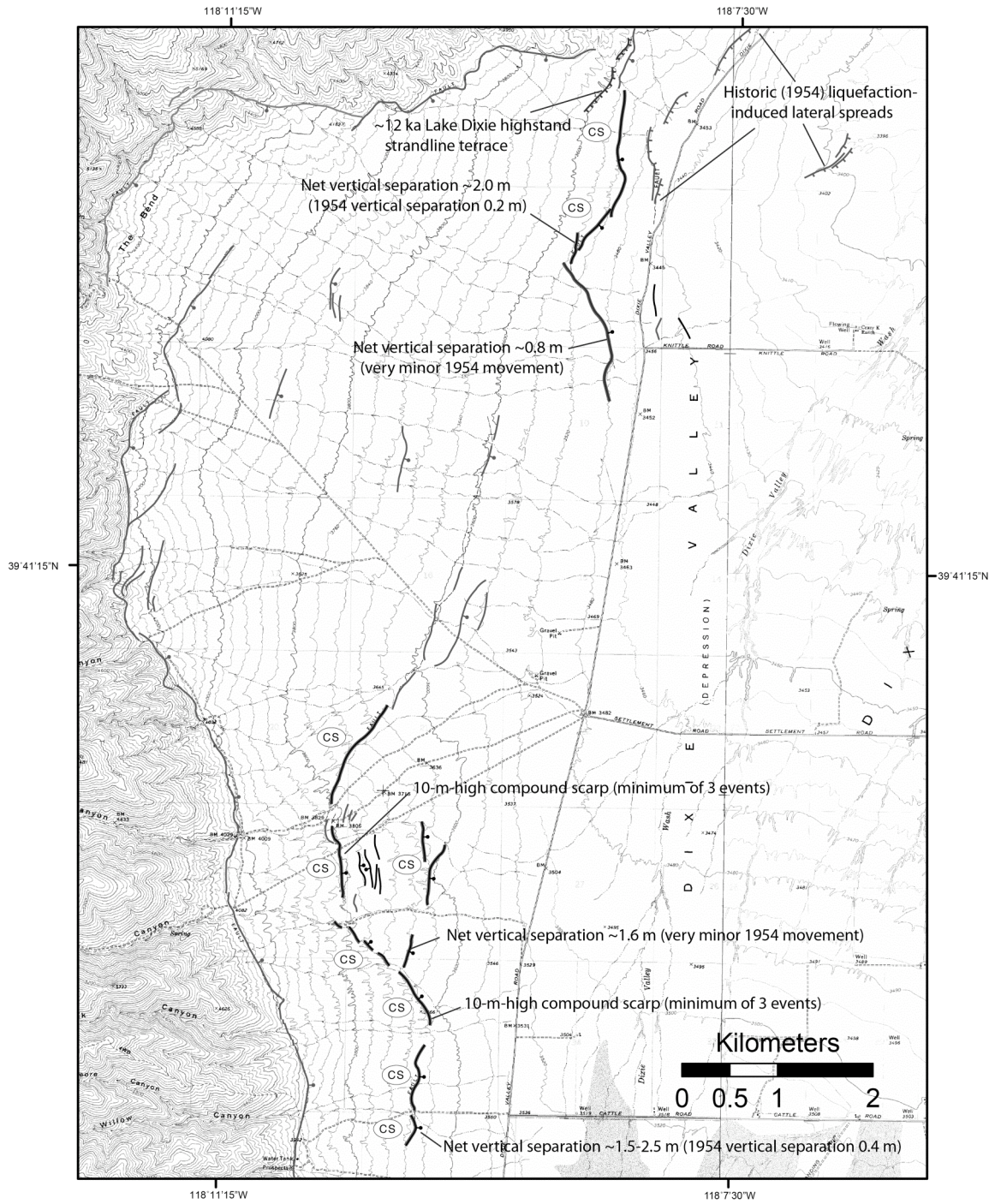
Historic liquefaction-induced lateral spread features formed during the 1954 Dixie Valley earthquake - hachers shown only on most prominently-expressed valley-facing headscarps. Most headscarps are accompanied by back-facing scarps across lateral-spread graben, which cannot be shown at this map scale.
- 

Paleo-liquefaction-induced lateral spread features formed during the ~2.5 ka "Gap event" - hachers shown only on most prominently-expressed headscarps (valley-side hachers) and back-facing scarps along lateral-spread graben. Non-hachered traces mainly represent lateral-spread fissures or smaller head scarps and back-facing scarps in areas of highly complex ground failures.
- 

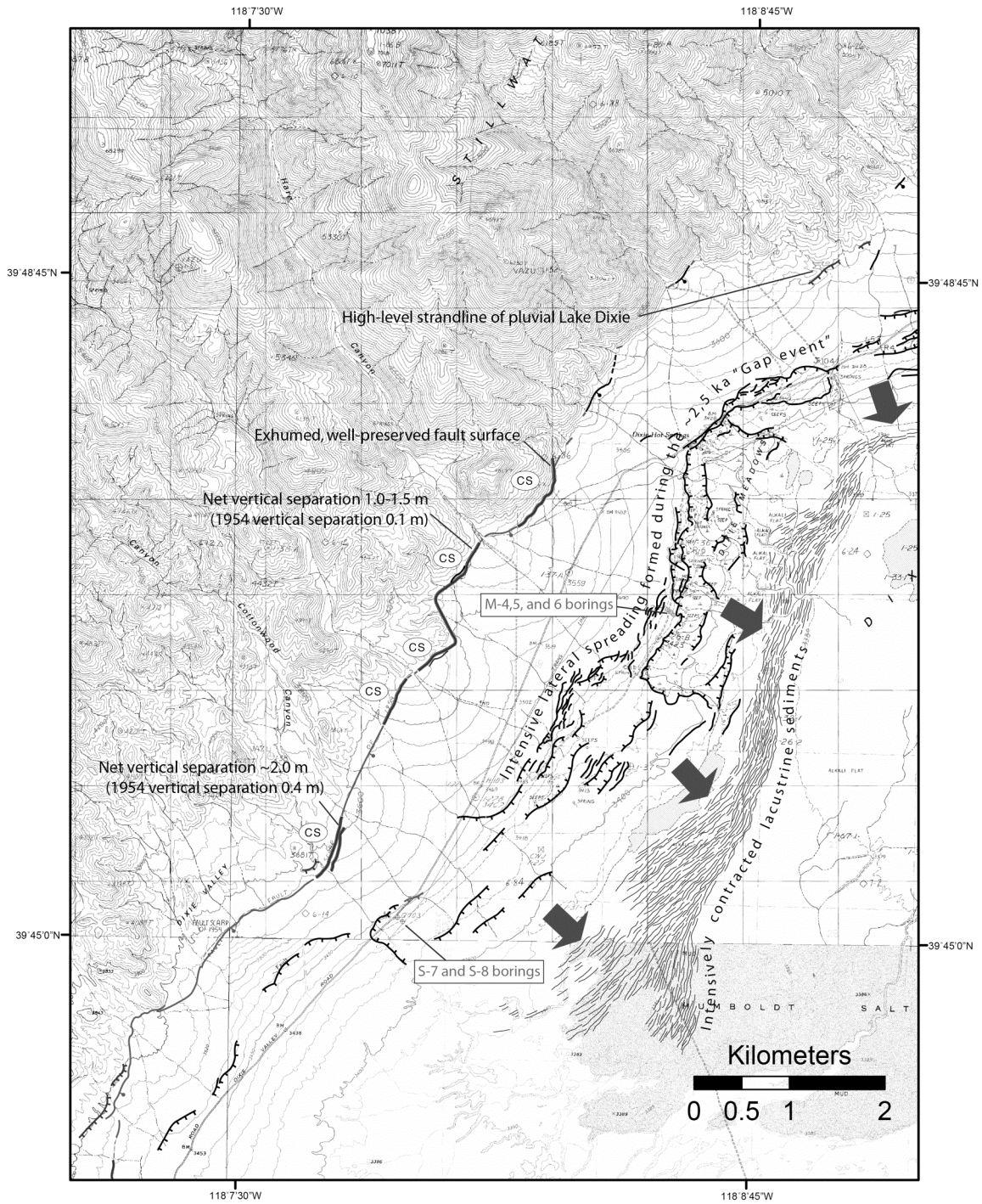
Map traces of contractional features formed at the down-slope terminations of paleo-lateral-spread-induced ground failures - lineations represent very shallowly-rooted folds and "faults." Contractional shortening directions are shown by bold arrows. These features are all interpreted to have formed during large-magnitude paleo-lateral spreading during the ~2.5 ka "Gap event".
- 

High-level Pluvial Lake Dixie shoreline features - hachers on lake side of map traces, which represent various types of shoreline features such as cemented beach-rock, ledges, strandline terraces, and shoreline gravel bars. Pluvial Lake Dixie reach a high stand elevation of ~1095 m (3600 ft) at approximately 12 ka (Thomson and Burke 19Bell et al., 2004)

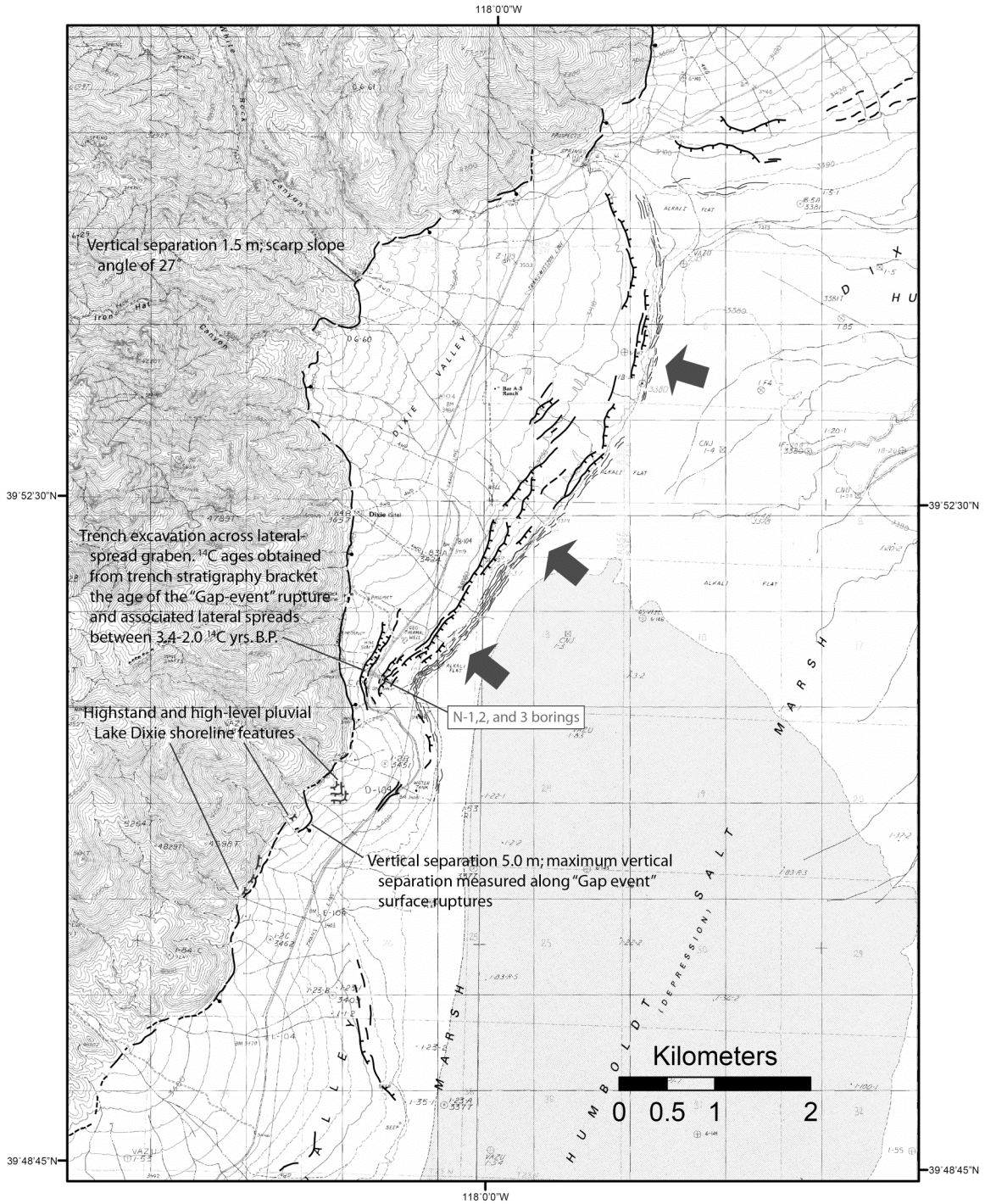
APPENDIX 1B.



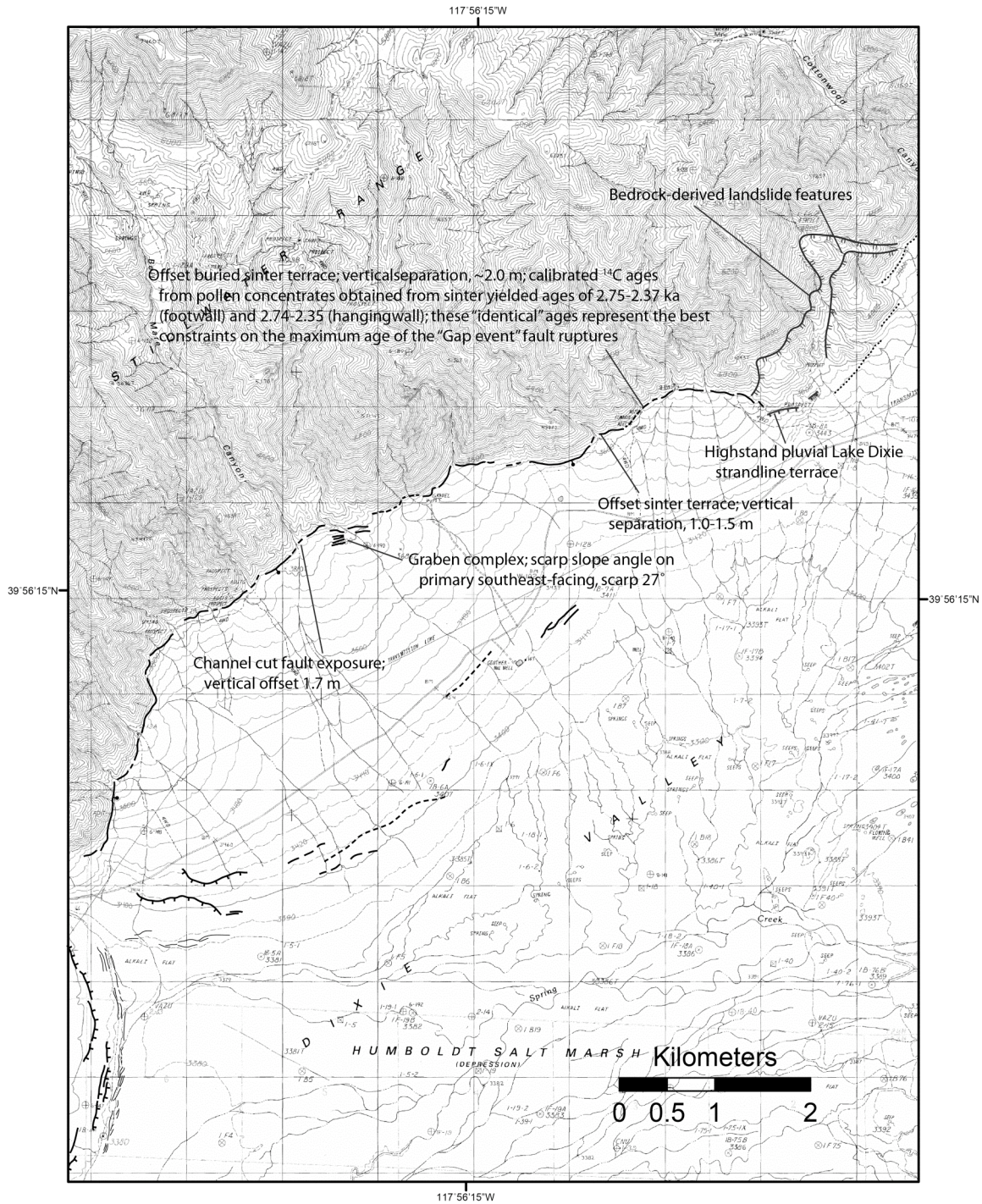
APPENDIX 1C.



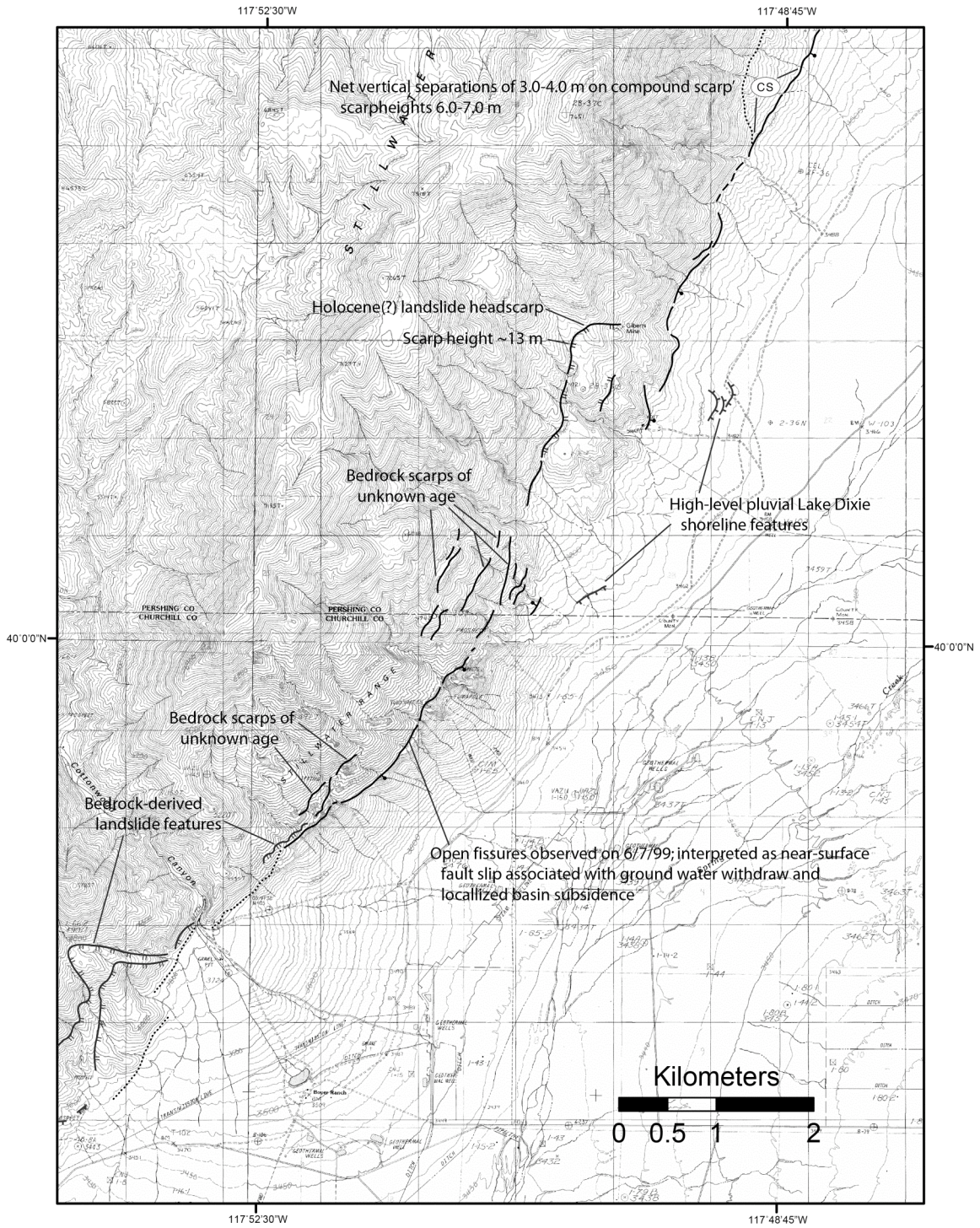
APPENDIX 1D.



APPENDIX 1E.



APPENDIX 1F.



APPENDIX 1G.

